

CORROSION-INDUCED FATIGUE PERFORMANCE OF S460 AND S690 HIGH-STRENGTH STEELS

^{1,*}Mohammad S. Al KHAZALI, ¹Petr MIARKA, ¹Lucie MALÍKOVÁ, ¹Stanislav SEITL

¹Faculty of Civil Engineering, Brno University of Technology, Veveří 331/95, 602 00 Brno, Czech Republic, EU, mohammad.sami.al.khazali@vutbr.cz

https://doi.org/10.37904/metal.2025.5127

Abstract

Although high-strength structural steels deliver excellent strength-to-weight ratios, their fatigue reliability drops sharply once corrosion pits develop. In this study, S460 specimens were corroded in controlled salt spray cycles. Pit geometry was measured using X-ray microCT and rotating bending tests were performed to establish *S–N* curves. A plane-strain finite-element model was used to convert pit depth into local stress-concentration factors, confirming that deeper pits, rather than nominal yield strength, govern endurance loss. The same corrosion and testing protocol were repeated on S690, and these data will be used to complete a grade-to-grade comparison in future work. The results highlight the need for early surface protection or fatigue design reductions that explicitly account for pit depth.

Keywords: Corrosion fatigue, high-strength steel, pit depth, stress concentration, finite-element modelling

1. INTRODUCTION

High-strength structural steels, such as S460 and S690, are widely used in the construction of bridges, cranes, and offshore towers, as their high yield-to-density ratios enable lighter, lower-carbon designs [1, 2]. When these steels operate in marine or industrial atmospheres, cyclic wetting and chloride deposition create micronscale pitting that transforms a nominally smooth surface into a field of sharper notches; the resulting stress amplification accelerates fatigue crack nucleation and growth [3-5]. Finite-element studies of corroded HSS specimens show that the local von Mises stress at a pit rim increases steadily with depth. Enlarging a pit from 0.1 mm to 1 mm, for example, increases the stress-concentration factor K_t by around a quarter [6]. This trend is also confirmed by σ_{yy} singularities along the ligament ahead of the pit [7].

These numerical findings are echoed by experimental work. Rotating-bending fatigue tests on S460 cylinders exposed to short periods of salt spray show a progressive downward shift in the S-N curve and increased scatter in the life data as the pits deepen. Similar observations on welded and non-welded HSS components suggest that pit morphology, rather than base-metal yield strength, governs endurance loss once corrosion begins [8]. Finite-element studies on corroded HSS specimens demonstrate that local von Mises stress at a pit rim increases steadily with depth. Enlarging a pit from 0.1 mm to 1 mm, for example, increases the stress-concentration factor K_t by approximately 25 %, a trend also confirmed by σ_{yy} singularities along the ligament ahead of the pit.

Despite this progress, most published datasets and calibrations focus on a single grade. A direct, side-by-side comparison of pit shape, K_t and fatigue response for S460 and the higher-strength S690 is still lacking [9, 10]. The present study addresses that gap by coupling μ -CT pit mapping, rotating-bending fatigue testing and plane-strain FEM on identically corroded S460 and S690 specimens. The resulting data set establishes that pit depth rather than nominal strength dictates fatigue degradation and provides a depth-based K_t curve to guide future corrosion-fatigue modelling of high-strength steels (HSS).



2. MATERIALS AND METHODS

The high-strength steels S460 and S690 were supplied as 25 mm hot-rolled plates. Hourglass specimens with a minimum diameter of 4 mm and a gauge length of 24 mm were machined along the rolling direction, adopting the geometry already used in earlier corrosion-fatigue studies on the same alloy family.

2.1 Corrosion conditioning

Four surface states were prepared:

- Roof-stored control (outdoor exposure, average RH around 70 %, and average wind speed was about 5 m/s with average temperature ranged from -5°C in winter to 30 °C in summer).
- 3-day salt spray: 5 % NaCl, 35 °C.
- 6-day salt spray: identical conditions extended to six days.
- Salt + heat cycle: 6 days at 35 °C followed by 3 days at 50 °C to accelerate pit growth.

The pit morphology was quantified using X-ray microCT. The TORATOM cone-beam setup used for all scans is shown in **Figure 1**.

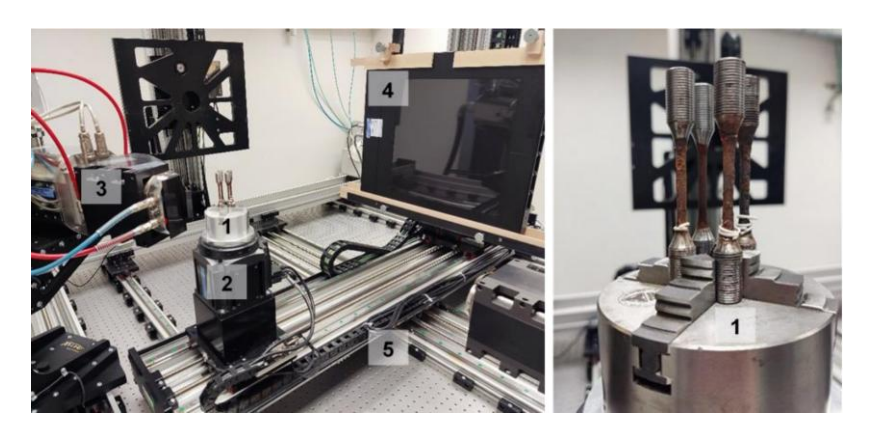


Figure 1 TORATOM tomography setup during data acquisition: (1) sample chuck, (2) rotating platform with a vertical rotation axis, (3) X-ray tube XWT-240-SE, (4) flat panel detector XRD 1611, (5) anti-vibration table with active vibration damping and CNC-controlled component movements

2.2 Fatigue testing

Fatigue tests were carried out under fully reversed loading (R = 0.1) at room temperature on standard round specimen $\phi 4$ mm. The resulting S-N curves for each corrosion condition are presented in **Figure 2**.



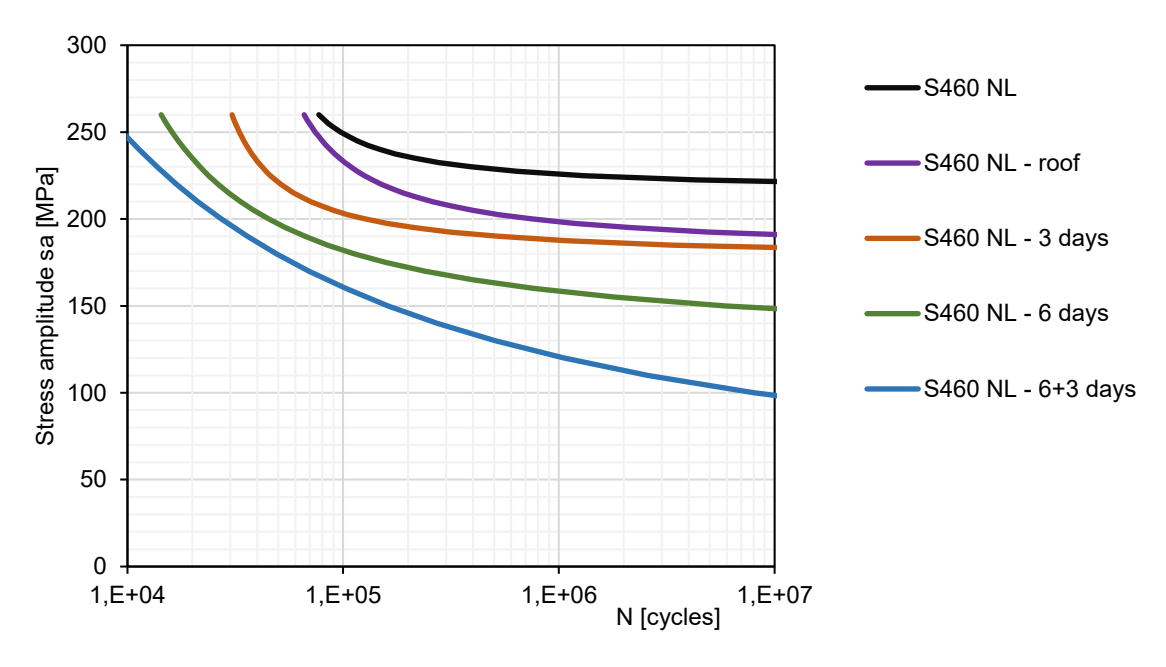


Figure 2 S-N curve for S460 under all corrosion conditions

2.3 Finite-element stress analysis

A two-dimensional plane-strain model after [11] was adopted to convert pit geometry into a stress-concentration factor.

- Geometry: a 4 mm-wide bar containing a semicircular pit with a depth ranging from 0.1 mm to 1.0 mm (as measured by μ-CT on the S460 specimens).
- Loading and boundary conditions: remote axial stress (σ_{remote}) = 100 MPa; symmetry constraints along the bar axis; the pit surface was left traction-free.
- Mesh: quadrilateral plane-strain elements refined to approximately 5 μm near the pit to ensure that the stress results are mesh-independent.
- The material data was linear elastic, with Young's modulus E = 210 GPa and Poisson's ratio = 0.30 for both the S460 (reference run) and the S690 (comparative run).
- The output metric was the peak von Mises stress ahead of the pit (called σ_{max}) divided by the applied remote stress σ_{remote} to obtain the stress-concentration factor: $K_t = \sigma_{max}/\sigma_{remote}$.

3.1 Corrosion morphology

To establish the geometric driver of fatigue degradation, we first quantified how pit depth and affected perimeter evolve under successive salt-spray exposures; **Table 1** and **Figures 3–4** distil the micro-CT evidence for both grades.



| Steel Type | Label | Condition | Max Defect Depth (μm) | % of Diameter Affected |
|------------|---------|-------------------------|-----------------------|---------------------------|
| S460 | S460_0D | Roof | 81.8 | 2.05 |
| S460 | S460_3D | 5% NaCl, 35°C | 346.2 | 8.65 |
| S460 | S460_6D | 5% NaCl, 35°C | 656.3 | 16.41 |
| S460 | S460_9D | 5% NaCl, 35°C + 50°C | 724.2 | 18.1 |
| S690 | S690_0D | Roof | 79.3 | 1.98 |
| S690 | S690_3D | 5% NaCl, 35°C | 139.8 | 7.31 |
| S690 | S690_6D | 5% NaCl, 35°C | 316.3 | 14.48 |
| S690 | S690_9D | 5% NaCl, 35°C + 50°C | 260.9 | 15.8 |

Table 1 Maximum pit depth D_{max} and pit-affected perimeter (%Ø) for S460 and S690

3.2 Fatigue performance

The S-N curves involving rotation and bending, which were introduced earlier in **Figure 2**, are now interpreted considering the pit statistics. Here, we demonstrate how each incremental increase in D_{max} (**Table 1**) corresponds to a systematic downward shift and steepening of the fatigue curve.

3.3 Pit-induced stress concentration

To link geometry with mechanics, we compare the finite-element $K_{t(D)}$ curve for S460 with the measured depth range. This analysis shows that pits deeper than approximately 0.5 mm increase K_t sufficiently to explain the loss of high-cycle life observed in Section 3.2.

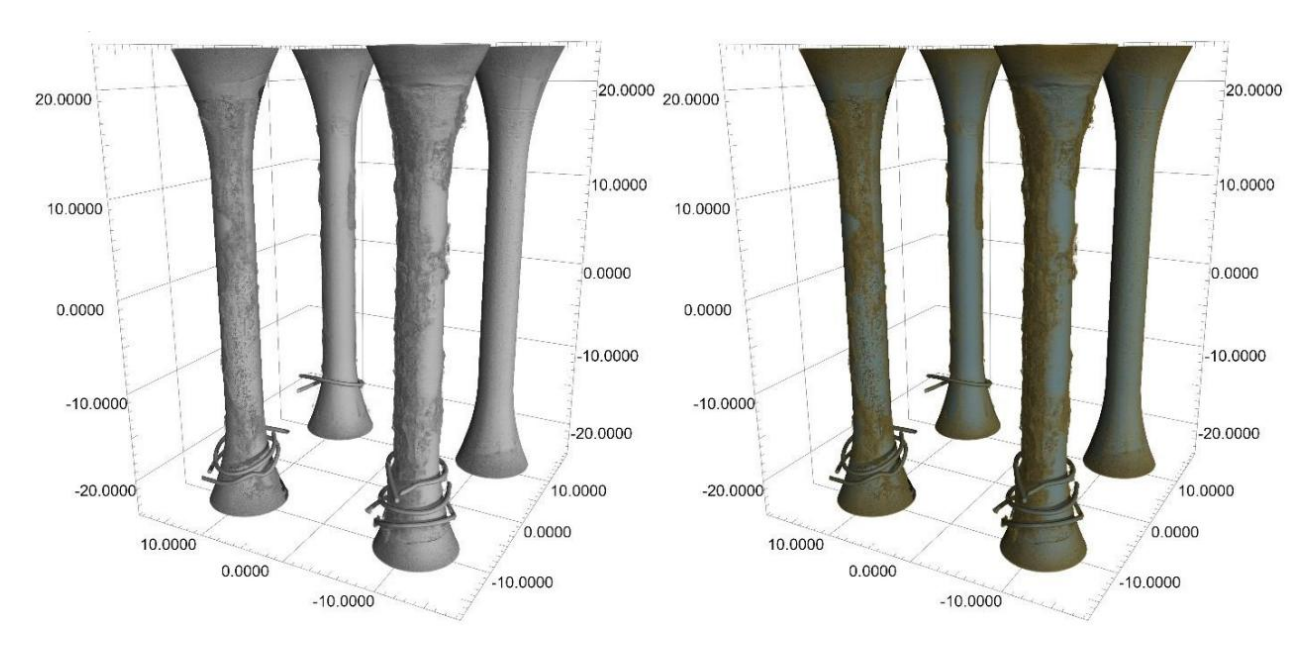


Figure 3 3D reconstruction of corrosion defects in S460; Left: three-dimensional grayscale visualization after tomographic reconstruction. Right: the same model with artificial colouring based on a threshold value, distinguishing between the original material (blue) and corrosion products (orange)



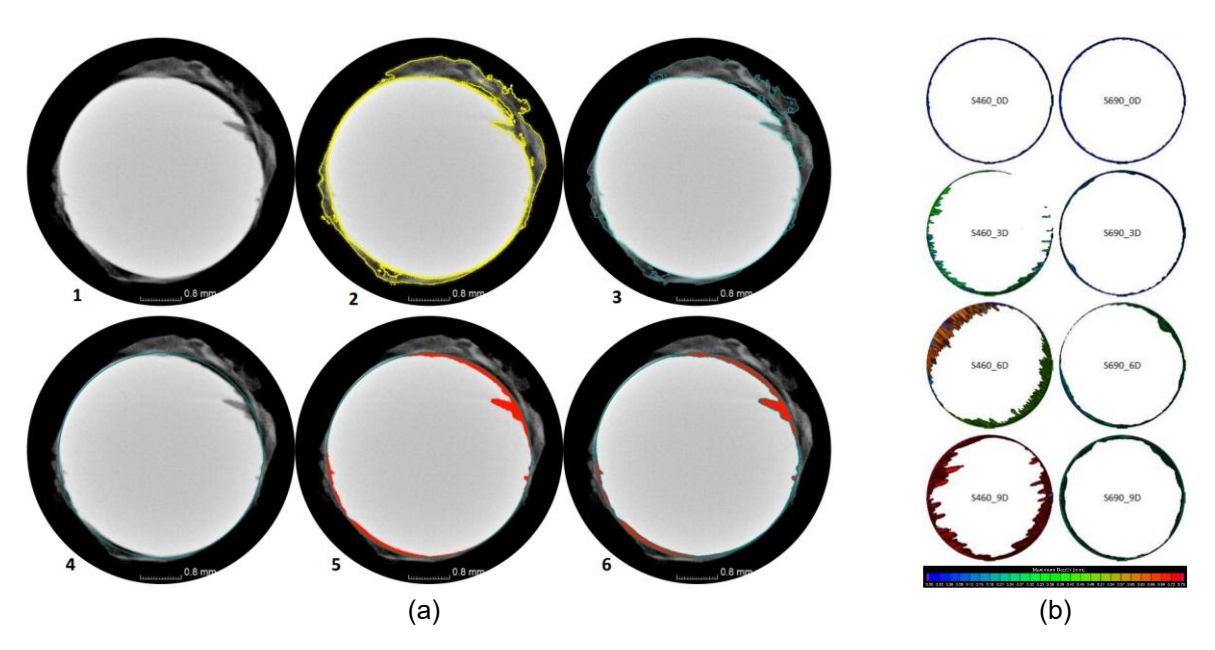


Figure 4 (a): 2D data processing for defect boundary detection; (1) Visualization of the central cross-section of S460_9D specimen, (2) Rough boundary marking for identifying intact material and corrosion (in yellow), (3) Precise boundary definition (in blue), (4) Reference cylinder boundary indicating the original material limits prior to corrosion exposure (in blue), (5) Damage detection through porosity analysis, (6) Definition of the radial extent of corrosion damage from the original surface of the specimen **(b)** 3D representation of corrosion damage for S460 and S690

3.4 Comparative FEM projection for S690

Finally, rerunning the identical mesh with S690 properties generates a grade-independent $K_{t(D)}$ curve (**Figure 5**). This provides a predictive baseline for the S690 fatigue data that is currently being analysed. **Figure 5** reproduces the elastic von-Mises stress distributions ahead of a semicircular surface pit obtained with the plane-strain model of [11]. For S460, the peak stress increases from approximately 155 MPa at D = 0.1 mm to approximately 325 MPa at D = 1.0 mm. This gives a stress-concentration factor of $K_t = \sigma_{max}/\sigma_{remote}$, which increases from 1.55 to 3.25.

Rerunning the identical mesh with a linear-elastic S690 card yields the same $\sigma_{\text{VM}(x)}$ family (difference <2%), because in linear elasticity, K_t depends only on pit geometry and not on yield strength. Therefore, the grade-independent K_D trend provides a predictive baseline for the S690 fatigue tests currently being processed. Once the data are available, **Figure 5** will serve as the benchmark for assessing depth-controlled endurance loss in the higher-strength steel.



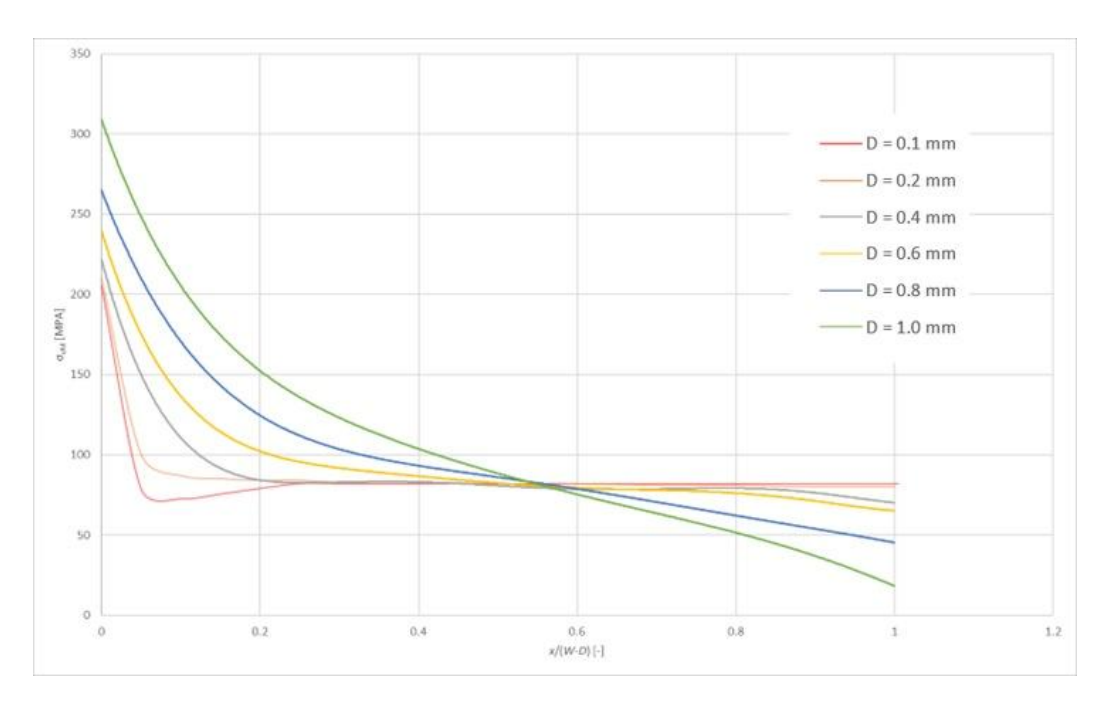


Figure 5 Elastic von Mises stress distributions in front of a semicircular pit of six different depths (D = 0.1 - 1.0 mm) in a 4 mm bar under plane strain loading at $\sigma_{\text{remote}} = 100 \text{ MPa}$ for S690

3. DISCUSSION & CONCLUSIONS

Pit depth dictates local stress: The elastic plane-strain model shows that K_t rises from approximately 1.5 to approximately 3.3 as the pit depth increases from 0.1 to 1.0 mm. This reproduces the trend observed by [11]. and matches our own rerun with an S690QL card. Since K_t is geometry-controlled in linear elasticity, nominal yield strength has no effect on stress amplification once a pit has formed. Rerunning the identical mesh with a linear-elastic S690 card produces the same $\sigma_{\text{VM}(x)}$ family (difference <2%), since K_t in linear elasticity depends only on pit geometry and not yield strength. Therefore, the grade-independent $K_{t(D)}$ trend provides a predictive baseline for the S690 fatigue tests that are currently being processed. Once that data is available, **Figure 5** will serve as the benchmark for assessing depth-controlled endurance loss in the higher-strength steel.

Surface damage scales endurance loss: The S460 S–N curves systematically shift downwards and steepen with the D_{max} values reported in **Table 1**. The largest depth (approximately 0.7 mm, or 18% \emptyset) coincides with a tenfold drop in high-cycle life, confirming that the $K_{t(D)}$ relation provides a direct link between pit geometry and fatigue knock-down.

Grade-independent projection for S690QL: As S690 shares the same $K_{t(D)}$ curve as S460NL, the forthcoming fatigue data for S690 are expected to follow the same depth-controlled life reduction. This validates the use of a unified pit-depth design check for both grades.

Practical implications: A rapid surface protection method or depth-based stress derating (for example, prohibiting pits deeper than 0.3 mm in 4 mm bars) is more effective than relying on higher nominal strength alone. The depth-to- K_t curve in **Figure 5** can be adopted directly in corrosion-fatigue assessment codes.

ACKNOWLEDGEMENTS

The research is supported by FAST-S-25-8839, Faculty of Civil Engineering, Brno University of Technology.



REFERENCES

- [1] Jiang, C., Wu, C. and Jiang, X. Experimental study on fatigue performance of corroded high-strength steel wires used in bridges. *Constr. Build Mater.* 2018, Vol. 187, pp. 681–690. doi: 10.1016/J.CONBUILDMAT.2018.07.249.
- [2] Qiang, X., Bijlaard, F. S. K. and Kolstein, H. Post-fire mechanical properties of high strength structural steels S460 and S690. *Eng. Struct.* 2012, Vol. 35, No. 2, pp. 1–10. doi: 10.1016/J.ENGSTRUCT.2011.11.005.
- [3] Balbín, J. A., Chaves, V. and Larrosa, N. O. Pit to crack transition and corrosion fatigue lifetime reduction estimations by means of a short crack microstructural model. *Corros. Sci.* 2021, Vol. 180, No. 3, p. 109171. doi: 10.1016/J.CORSCI.2020.109171.
- [4] Hollý, I. and Bilcik, J. Effect of chloride-induced steel corrosion on working life of concrete structures. *Solid State Phenomena*. 2028, Vol. 272, pp. 226–231. doi: 10.4028/WWW.SCIENTIFIC.NET/SSP.272.226.
- [5] Cai, J., Sun, L., Ma, H. and Li, X. Corrosion characteristics of Q690qE high-strength bridge steel in simulated coastal–industrial environment and its influence on mechanical and corrosion fatigue behaviors. *Constr. Build. Mater.* 2022, Vol. 341, No. 6, p. 127830. doi: 10.1016/J.CONBUILDMAT.2022.127830.
- [6] Mu, Z. T., Chen, D. H., Zhu, Z. T. and Ye, B. The stress concentration factor with different shapes of corrosion pits. Adv. Mat. Res. 2011, Vol. 152–153, pp. 1115–1119. doi: 10.4028/WWW.SCIENTIFIC.NET/AMR.152-153.1115.
- [7] Yan, W., Guan, L., Xu, Y. and Deng, J. G. Numerical simulation of the double pits stress concentration in a curved casing inner surface. *Advances in Mechanical Engineering*. 2016, Vol. 9, No. 1. doi: 10.1177/1687814016682652.
- [8] Zhang, H. et al. Fatigue behavior of high-strength steel wires considering coupled effect of multiple corrosion-pitting. *Corros. Sci.*, 2025, Vol. 244, No. 3, 112633. doi: 10.1016/J.CORSCI.2024.112633.
- [9] Mokhtari, E., Heidarpour, A. and Javidan, F. Mechanical performance of high strength steel under corrosion: A review study. *J. Constr. Steel Res.* 2024, Vol. 220, No. 9, p. 108840. doi: 10.1016/J.JCSR.2024.108840.
- [10] Guo, Z., Ma, Y., Wang, L., Zhang, J. and Harik, I. E. Corrosion Fatigue Crack Propagation Mechanism of High-Strength Steel Bar in Various Environments. *Journal of Materials in Civil Engineering*. 2020, Vol. 32, No. 6, p. 3165. doi: 10.1061/(ASCE)MT.1943-5533.0003165.
- [11] Malíková, L., Benešová, A., Al Khazali, M. S., Křivý, V. and Seitl, S. Stress Concentration Factor on a Corrosion Pit. Sborník vědeckých prací Vysoké školy báňské Technické univerzity Ostrava. Řada stavební. 2023, Vol. 23, No. 2, pp. 27–30.